Accepted Manuscript

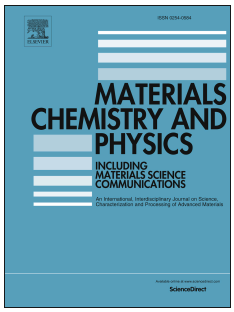

Mesoporous metal oxide/pyrophosphate hybrid originated from reutilization of water treatment resin as a novel fire hazard suppressant

Ye-Tang Pan, Miguel Castillo-Rodríguez, De-Yi Wang

PII: S0254-0584(17)30742-3

DOI: 10.1016/j.matchemphys.2017.09.040

Reference: MAC 20007

To appear in: *Materials Chemistry and Physics*

Please cite this article as: Ye-Tang Pan, Miguel Castillo-Rodríguez, De-Yi Wang, Mesoporous metal oxide or pyrophosphate hybrid originated from reutilization of water treatment resin as a novel fire hazard suppressant, *Materials Chemistry and Physics* (2017), doi: 10.1016/j.matchemphys.2017.09.040

- Mesoporous $SnO_2/Ca_2P_2O_7$ hybrid (TCP) was derived from waste chelating resin.
- TCP reduced corrosive HCl release from flexible PVC composite during combustion.
- Flexible PVC composite with TCP show good smoke suppression and flame retardancy.
- TCP has the great potential to replace harmful antimony trioxide as flame retardant.

Mesoporous metal oxide/pyrophosphate hybrid originated from reutilization of water treatment resin as a novel fire hazard suppressant

Ye-Tang Pan, Miguel Castillo-Rodríguez and De-Yi Wang*

IMDEA Materials Institute, C/Eric Kandel, 2, 28906 Getafe, Madrid, Spain.

*Corresponding author: De-Yi Wang. E-mail address: deyi.wang@imdea.org. Tel.: +34 915493422-1055.

ABSTRACT: Flexible poly(vinyl chloride) (fPVC) composites undertake potential high fire and smoke hazards. Withal, commercial flame retardant, antimony trioxide (Sb_2O_3), in application to fPVC is proved to be harmful anyhow. Meanwhile, corrosive HCl gas evolves inevitably from fPVC during combustion. In this article, mesoporous $SnO_2/Ca_2P_2O_7$ hybrid crystals with high specific surface area and pore volume was firstly synthesized via a facile way by utilization of the chelating resin as the precursor. The composition and structure of the hybrid material were characterized by X-ray diffraction, scanning electron microscope/transmission electron microscope coupled with energy dispersive X-ray detector and N_2 sorption isotherms. The results from limiting oxygen index, vertical burning test and cone calorimeter showed that the synthesized product reduced the fire and smoke hazards of fPVC and decreased the amount of HCl gas emission due to the combined impact of SnO_2 and $Ca_2P_2O_7$. Moreover, this novel flame retardant holds great potential to replace antimony trioxide and provides the promising manner to develop Sb_2O_3-free environmental friendly fPVC composite with low fire hazards.

KEYWORDS: *flexible poly(vinyl chloride)**;** smoke suppression; HCl removal; flame retardancy*

1. Introduction

Poly(vinyl chloride) (PVC) is a type of universal synthetic plastic, widely used in various fields [1]. Among these applications, flexible forms of PVC occupy a high proportion. Generally, pristine PVC is regarded as no-combustion resin under normal circumstances [2]. However, the introduction of plasticizers augments the fire hazard of flexible poly(vinyl chloride) (fPVC). It divulges that the flame retardancy of flexible products is extremely inferior to the rigid ones [3]. It is recognized that fire hazards of polymeric materials consist of thermal and smoke risks [4-6]. The underlying smoke hazards of fPVC pose a serious threat to human beings, since choking smoke poisoning is the leading cause of fire deaths [7]. According to the current report, fire smoke toxicity of PVC was discerned to be the most toxic among all the investigated polymers [8]. Meanwhile hydrogen chloride (HCl) gas is also released from PVC in the course of combustion. This inorganic irritant exacerbates the stimulating and stifling results of the smoke [9]. Antimony trioxide (Sb_2O_3) has been exploited as traditional flame retardant for fPVC, but antimony compounds were proved to be harmful [10, 11]. Nowadays, inorganic tin compounds are assumed to be one of the most suitable candidates to substitute Sb_2O_3 [3, 12-14].

The content of calcium is one of the key parameters to determine the hardness of groundwater [15]. The high hardness of groundwater caused by the existence of plentiful calcium deteriorates its practical application. The most common methods for removal of extra metal ions are the usage of resins or chemical precipitation [16].

Macroporous chelating resin D402 with poly(styrene-divinylbenzene) as matrix and aminophosphonic acid as active site provides outstanding ability of coordination with metal ions, especially these divalent ones including Ca^{2+}. Howbeit, after several rounds of recycling, regeneration and reutilization, Ca-rich resin is not able to be further used and its disposal appears to be a challenging problem. Interestingly, copious amount of phosphorous in the waste resin is to generate in the burning process, a compact and integrated barrier intrinsically consist of polyphosphoric acid and to motivate the behavior of intumescence [17]. Since basic salt has the potential to react HCl thus reduce the amount of effluent, reminiscent of calcium carbonate that is proved to be considerably effective as filler for removal of HCl decomposed from PVC according to the previous report. Inspired by this, the waste resin can be converted into calcium pyrophosphate ($Ca_2P_2O_7$) via several steps afterwards reduce HCl amount evolved from PVC during combustion and improve flame retardancy of the PVC composite simultaneously [18, 19]. In addition, thanks to the abundant pores in the carbonized resin, the facile loading of tin oxide (SnO_2) in the hybrid enables the flame retardancy of the composite to be further enhanced.

In an attempt to reduce fire hazards, suppress smoke, decrease corrosive HCl release and replace harmful Sb_2O_3 for fPVC composite, mesoporous $Ca_2P_2O_7$ was synthesized through carbonization and calcination, in the meantime, tin element was introduced into the system via incipient wetness impregnation within the procedure in this study. Such sustainable engineering method has generality to fabricate $MO_x/M_yP_2O_7$ by means of

choosing different adsorbed/chelated initial metal ions. It is anticipated that the as-synthesized robust material (donated as TCP) with high specific surface area and pore volume could exhibit high performance in fPVC composite during combustion, thus leading to improved fire safety in practical application.

2. Experimental sections

2.1. Materials

D402-II chelating resin was provided by Jiangsu Suqing Water Treatment Engineering Group Co., Ltd. Calcium bicarbonate solution [$Ca(HCO_3)_2$] (98.5%), tin (IV) chloride ($SnCl_4$) and trioctyl trimellitate (TOTM) were bought from Sigma Aldrich. PVC resin with K=70, thermal stabilizer (calcium-zinc stearate mixtures), epoxidized soybean oil, wax (polyethylene) and Sb_2O_3 were supplied by Quimidroga, s.a.

2.2. Synthesis of SnO_2/$Ca_2P_2O_7$ hybrid material (TCP)

Firstly, 1 g $Ca(HCO_3)_2$ solution was dropped into 400 ml deionized water and stirred sufficiently for 1 h. Then 3 g D402-II macroporous chelating resin was poured into the solution and stirred mildly for another 2 h. The Ca-doped resin was filtered followed by washing with de-ionized water three times and completely drying in the oven at 80 °C overnight. Afterwards, Ca-doped carbonized resin was prepared by utilizing pillar effect according to the literature [20]. The divalent cations could form ionic crosslinking connecting two or three functional groups in the resins. The crosslinking functional groups and cations were converted to highly dispersed metal salts or elemental metals during the carbonization, which would form a kind of pillar to maintain pores in the

carbonized resins. In a typical run, Ca-doped resin placed on a combustion boat were carbonized in a horizontal tubular furnace in the nitrogen stream of 300 cm^3/min at the rate of 10 K/min up to 700 °C at which they were kept for 10 min. After that, the fabrication of porous carbonized resin functionalized with Sn^{4+} within the cavity was accomplished by incipient wetness impregnation employing a tin chloride aqueous solution based on the weight ratio of 90 g $SnCl_4$ to 100 g water. 1 g solution was utilized to soak 2 g carbonized resin. Then the product was dried and calcined at 800 °C in a muffle furnace for 5 h. Finally, the particles were milled into powders by high-energy planetary mill at 300 rpm for 30 min. The final product was donated with the name TCP. The details about the synthetic process were sketched in Scheme 1.

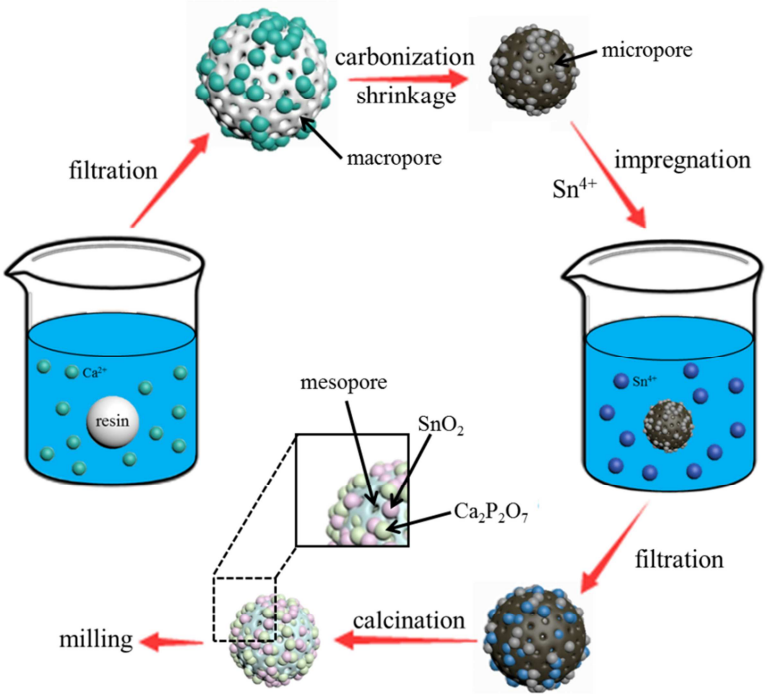

Scheme 1. Procedure for the preparation of the hybrid material.

2.3. Process of flexible PVC composites

Flexible PVC composite comprises 100 g PVC resin, 35 g trioctyl trimellitate, 7.5 g thermal stabilizer (calcium-zinc stearate mixtures), 5 g epoxidized soybean oil, 0.2 g wax and 5 g (3.2 wt.%) flame retardant (Sb_2O_3 and TCP). The neat PVC resin with additives was blended first and then extruded by a twin-screw extruder system (KETSE 20/40 EC, Brabender). The working temperature was 175 °C and the screw speed was at around 75 rpm. The pellets after cutting were added into injection molding machine (Arburg 320 C) at 175 °C to obtain the specimens with proper shapes for LOI and cone calorimeter tests. For the vertical burning test, the specimens were prepared by hot-plate press (LabPro 400, Fontijne Presses) at 175 °C.

2.4. Measurements

The powder X-ray diffraction (XRD) was carried out by Philip X' Pert PRO diffractometer with a Cu Kα tube and Ni filter (λ = 0.15405 nm). The voltage and current was 45 kV and 40 mA, respectively. Microstructures of the as-synthesized materials, fractured surface of the composite and the char layers after burning were studied using a scanning electron microscope (SEM, EVO MA15 Zeiss) equipped with energy dispersive X-ray detector (EDX). N_2 sorption isotherms were recorded on a Micromeritics instrument (ASAP 2010). Brauner-Emmett-Teller (BET) equation and Barrett-Joyner-Halenda (BJH) model were applied to acquire the specific surface area and the pore size distribution, correspondingly. Transmission electron microscope (TEM) was carried out in a FE6 S/TEM microscope (Talos F200X, FEI) equipped with a chemical analysis via energy-dispersive X-ray spectroscopy operating at 80 kV.

Thermogravimetric analysis (TGA) was recorded from room temperature to 800 °C. The heating rate was 10 °C per minute in nitrogen gas and the flow speed was 90 ml per minute by means of a TA Q50 thermogravimetric analyzer. Limiting oxygen index (LOI) was determined with specimens (120 × 6.5 × 3 mm^3) based on the standard of ASTM D 2863-77. The vertical burning test (UL-94) was implemented with the help of a vertical burning instrument (Fire Testing Technology, UK). The tested samples were of sizes 130 × 13 × 0.6 mm^3 films. Fire hazards of samples in a forced-flaming situation were studied by FTT Cone Calorimeter according to ISO5660. The exterior heat flux of 50 kW/m^2 with shape of 100 × 100 × 4 mm^3. During the test, the HCl gas containing in the emitting gas of each sample from cone calorimeter machine was collected by the facility depicted in Fig. 1. The Cl^- concentration in the aqueous solution was measured by DIONEX ion chromatograph DX-500 with conductimetric and amperometric detector, composed of module columns guard, and analytical auto suppressors LC 20, module GP 40 gradient pump, ED 40 electrochemical detection module and AS 40 automatic sampler.

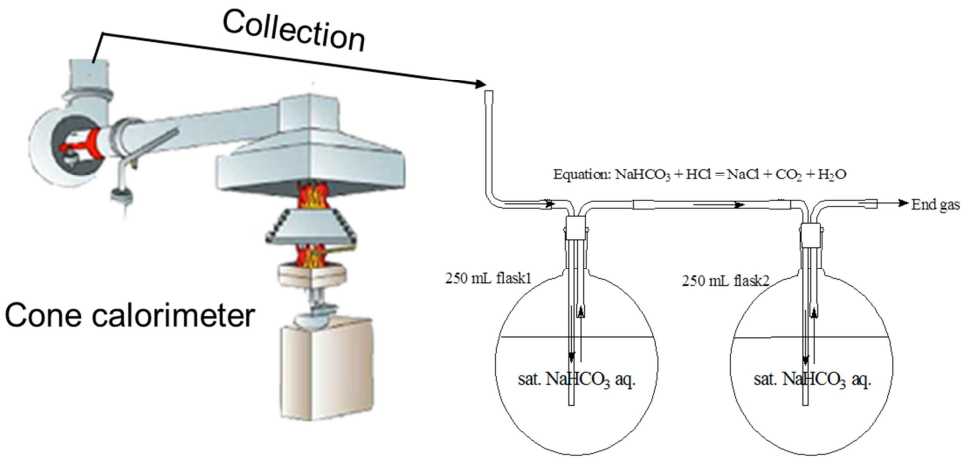

Fig. 1 Schematic diagram of HCl gas adsorption during cone calorimeter test.

3. Results and discussion

3.1. Characterization of TCP

According to XRD pattern (Fig. 2), the product was composed of two components: calcium phosphate oxide ($Ca_2P_2O_7$) with PDF card number 001-0667 (JCPDS) and cassiterite (SnO_2) with PDF card number 070-4177. The presence of $Ca_2P_2O_7$ illuminated that the conversion from coordinated calcium to calcium pyrophosphate was completed through carbonization, and the residual carbon as by-product was removed through calcination. During the carbonization, the macropores in the resin shrinked into micropores resulting in higher specific surface area and larger pore volume of the product which was beneficial to the adsorption of tin element into the cavity [16].

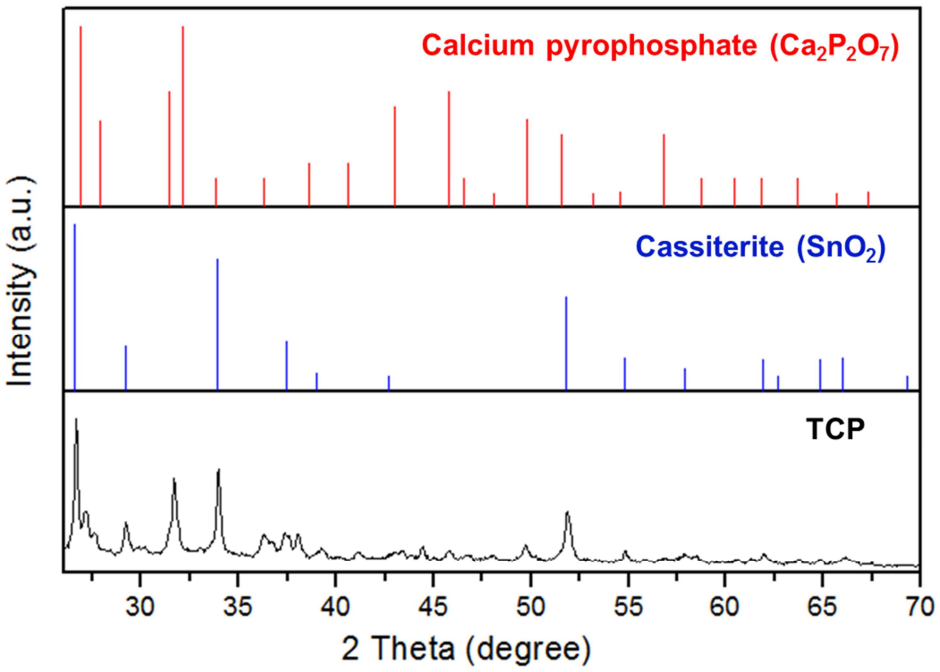

Fig. 2 XRD pattern of as-synthesized sample.

The morphology and composition of as-synthesized final product (after milling into fine powders) were detected by SEM/TEM and the results were shown in Fig. 3. As

could be observed in the SEM image (Fig. 3a), the product presented irregular shapes and the average grain size of the product was smaller than 500 nm. The morphology and elemental analysis were further studied by TEM. In the low magnification TEM image (Fig. 3b), the particle possessed dimension in submicron range, consistent with the result disclosed by SEM. The lattice fringes in the high-resolution TEM (Fig. 3d) can be ascribed to SnO_2 and $Ca_2P_2O_7$, respectively. Meanwhile, the lattice mismatch between the two components happened in the hybrid, probably caused by the high-temperature heat treatment during calcination. The distinct and individual spots in selected area electron diffraction (SAED) discerned in Fig. 3e provided the evidence that the hybrid was the mixture of two single crystals, namely the bright spots were ascribed to $Ca_2P_2O_7$ while the darker ones, observed from the inset of Fig. 3e, were belonged to SnO_2. The elemental analysis was also accomplished by the accessary energy dispersive X-ray detector of TEM, and the spectra were shown in Fig. 3f. The calcium, phosphorous and tin elements existed in the hybrid without any other impurities. The atomic ratio of calcium was close to that of phosphorous, in accordance with the stoichiometric proportion of $Ca_2P_2O_7$. The molar ratio of $Ca_2P_2O_7$ to SnO_2 in the hybrid calculated from the atomic ratio of calcium to tin was nearly 2.35 : 1. Apart from the EDX, the elemental mapping was also collected. From Fig. 3g, the calcium and phosphorous were well distributed all over the particle with nearly the same intensity, while tin element sporadically scattered in the particle with some level of agglomeration.

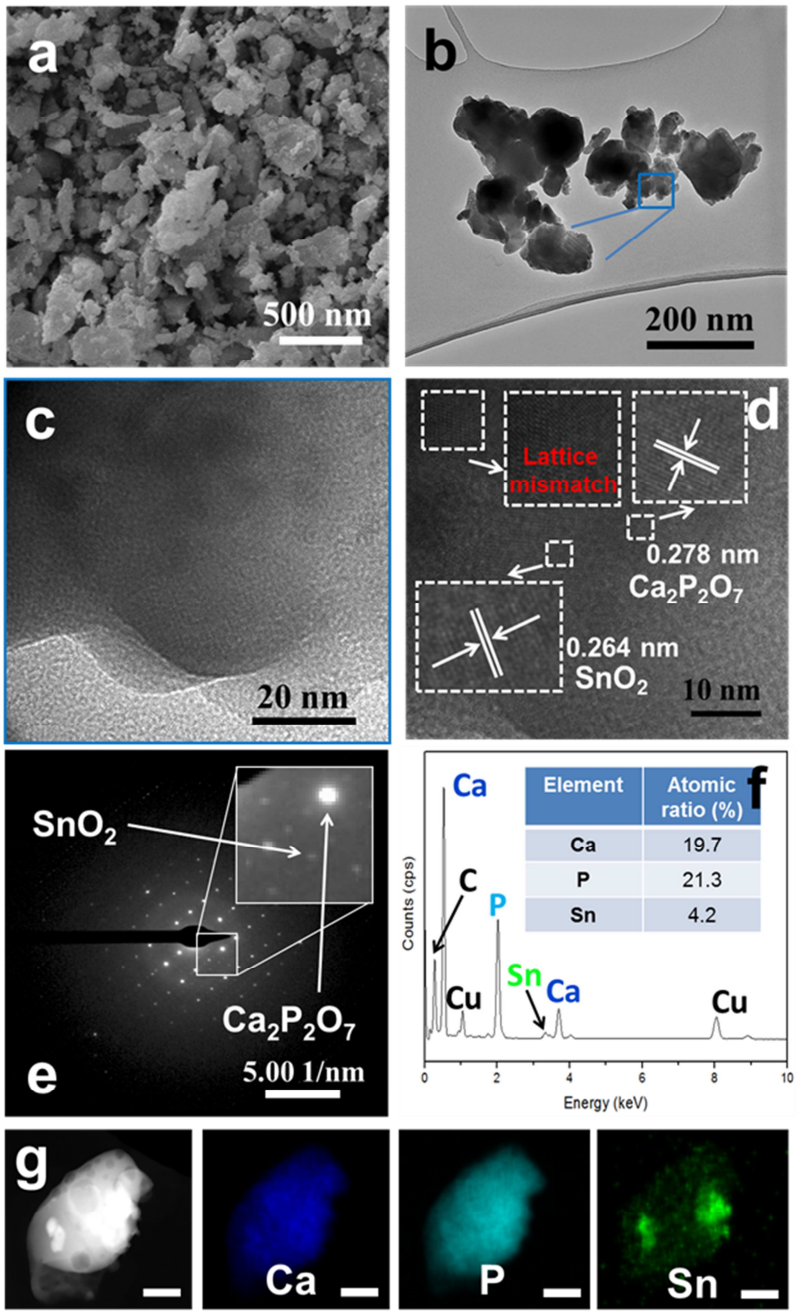

Fig. 3 (a) SEM image; (b) Low magnification TEM image; (c) Enlarged TEM image; (d) High-resolution TEM (HRTEM); (e) Selected area electron diffraction (SAED); (f) Energy dispersive X-ray spectra from TEM; (g) HAADF-STEM image and elemental mapping for final product with milling into fine powders (scale bar: 100 nm).

The prominent benefit for the aforementioned disposal of chelating resin was

providing a broad range of possibilities to confer the product with large BET surface area, multiple pores and large pore volume. In this article, corresponding properties of TCP were discerned by N_2 sorption isotherms and pore size distribution depicted in Fig. 4. According to the graph, a remarkable hysteresis loop emerged at relative pressure $p/p_0 > 0.4$ giving evidence that the N_2 adsorption-desorption process of TCP was ascribed to well-defined type-IV isotherms, which proved mesoporous structure existing in the sample. Likewise, the pore size distribution showed the mean aperture dimension was 2.1 nm within the range of mesopores. The existence of mesopores could be deduced that annealing process removed the residual carbon in the system thereby the pore size increased slightly from micropores to mesopores. In addition, the specific surface area and pore volume of TCP were 122 m^2/g and 0.124 cm^3/g correspondingly, predicting its high performance in the composite. The dispersion state and interfacial interaction of flexible PVC/TCP composite were investigated by fractured surface image obtained from SEM. From the SEM image (Fig. 4b), it can be seen that the TCP particles resided in the polymer. The porous feature of TCP facilitated strong interfacial adhesion and interaction between TCP and PVC matrix. There was no obvious agglomeration of TCP particles found in fractured surface, indicating good dispersion of TCP particles in flexible PVC matrix.

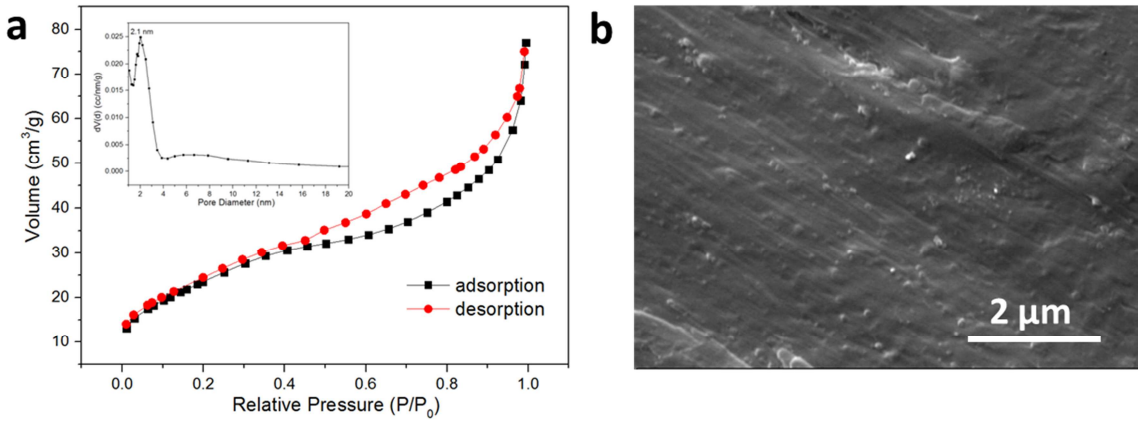

Fig. 4 (a) N_2 sorption isotherms and pore size distribution (inset) for TCP; (b) SEM image of fractured surface of fPVC/TCP composite.

The preparation process for TCP is discussed below in details. The SEM images of raw resin were shown in Fig. 5a, and the morphology of original resin was quite different from the final milled product. The resin possessed spherical shape with average particle diameter of 500 µm. The surface of the resin was relatively smooth decorated by several pores. The EDX spectra corroborated the existence of sodium and phosphorous elements in the system, which was consistent with the chemical formula of the raw resin. After chelating with Ca^{2+}, the particle size remained the same as the previous resin shown in Fig. 5b, however, the surface of the resin was broken due to the vigorous mechanical stirring. The stack of some small particles was detected in the broken area. The elemental analysis showed the Ca ion was successfully chelated by the resin while the Na element was disappeared. After carbonizing in inert atmosphere, the Ca-resin was transferred into $Ca_2P_2O_7$ and graphitic carbon (derived from the carbon skeleton of the resin), evidenced by XRD pattern (Fig. 5c) in which a sharp peak emerged at 2 theta = 26° attributing to (002) diffraction of graphitic carbon and all the

other peaks were indexed to $Ca_2P_2O_7$ [21, 22]. The particle size of the resin shrinked remarkably because of the collapse of organic framework in the system and the diameter of the spheres changed into 300 μm in average. Correspondingly, the macropores of the pristine resin also contracted into micropores indicated by the type-I isotherm in N_2 sorption measurement, conducive to the adsorption of tin ion into the aperture. Meanwhile, the smooth surface became rough with many small granules after carbonization. The carbonized resin was able to adsorb tin ion with a little amount of Cl ion which was proved by the EDX spectra in Fig. 5d. In the final step, the tin-calcium-doped resin was annealed in air and thus-obtained product transformed into loose and fragile balls with little shrinkage (Fig. 5e). The SEM image inside one broken ball exhibited the incompact and porous structure of the final product. The CO_2 formed by above mentioned graphitic carbon escaping from the system conferred the loose structure for the material with pore size extension from micrometric to mesometric. From EDX spectra of the specimen, Cl ion was removed by heat treatment and the ultimate elements in the product were calcium, phosphorous and tin. Meanwhile, the atomic ratio of the three elements retained nearly the same as the results gathered from TEM for the milling one. Moreover, the elemental mapping was also carried out, disclosing the uniform distribution of the three elements in the particle. Finally, the spheres were milled into fine powders (TCP) and then blended into PVC composite.

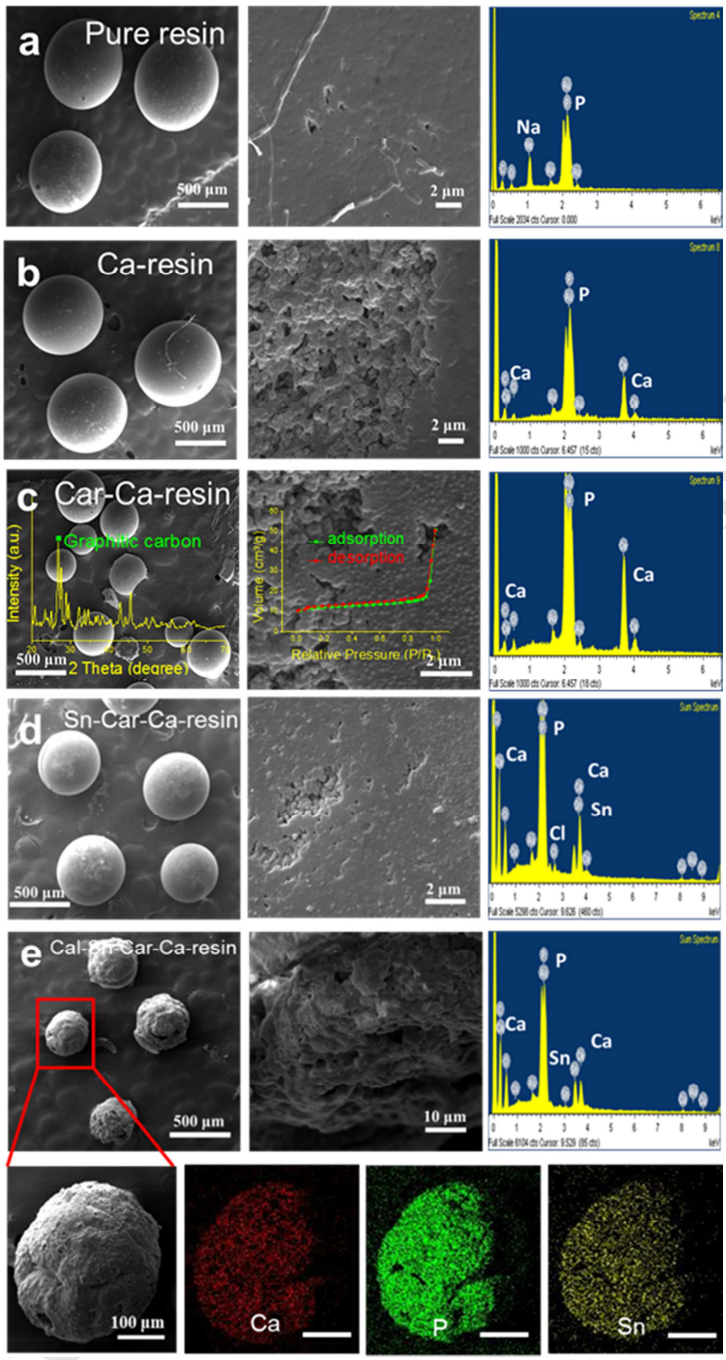

Fig. 5 (a) SEM graphics with EDX spectra of pure resin; (b) SEM graphics with EDX spectra of Ca chelated resin; (c) SEM images, XRD pattern, N_2 sorption isotherms and EDX spectra of Ca chelated resin after carbonization (Car-Ca-resin); (d) SEM graphics with EDX spectra of tin doped Car-Ca-resin (Sn-Car-Ca-resin); (e) SEM images, EDX spectra and elemental mapping of Sn-Car-Ca-resin after calcination (TCP before

milling).

3.2. Thermal stability of flexible PVC composites

TGA is generally accepted techniques for fast estimate of the thermal stability for multiple polymeric materials [23]. The profiles of flexible PVC composites were displayed in Fig. 6, and the relative results were listed in Table 1. The onset decomposition temperature ($T_{5\%}$) is defined as the temperature at 5 wt.% weight loss, while the temperature of the maximum mass loss rate (T_{max}) is termed as the temperature when the specimens exhibit the highest mass loss rate (MMLR).

The thermal degradation of flexible PVC composites was separated into two steps [24-27]. In presence of Sb_2O_3, the onset decomposition temperature was a little higher than that of untreated fPVC. Conversely, with the addition of TCP, $T_{5\%}$ of the composite was slightly decreased by 12 °C compared with pure fPVC. At the beginning of dehydrochlorination process, a few part of HCl was trapped by tin oxide to generate the strong Lewis acid-tin chloride. Such Lewis acid catalyzed the decomposition of fPVC, promoting early cross-linking and char layer formation. Meanwhile, the HCl reacted with $Ca_2P_2O_7$ to form polyphosphoric acid which was strong dehydration agent for polymer, beneficial to further char formation. Considering the char residue at 780 °C, Sb_2O_3-treated sample had the similar amount with the control sample (15.4 wt.%), which meant the addition of Sb_2O_3 did not influence the decomposition of fPVC, while the relatively high residue amount of TCP-treated sample (21.2 wt.%) implied that the introduction of TCP reduced the generation temperature of char barrier to prevent fPVC

composites from further pyrolysis.

With the regard to the DTG profiles, various interesting phenomena were revealed. Notably, the temperature of the maximal mass loss rate (T_{max1}) at first stage for fPVC/TCP was the highest among all the samples while the MMLR was the lowest. Yet based on the previous report, SnO_2 caused T_{max1} to happen in advance and had higher MMLR in comparison with those of pristine fPVC [3]. The reason was attributed to the integration of $Ca_2P_2O_7$ which contributed to stabilize the fPVC composite. The basic salts have the ability to shift the peak temperature (T_{max}) of dehydrochlorination to a higher temperature and decrease the rate of mass loss [18]. Therefore, the combination of SnO_2 and $Ca_2P_2O_7$ was able to improve the thermal stability of fPVC and facilitated char forming.

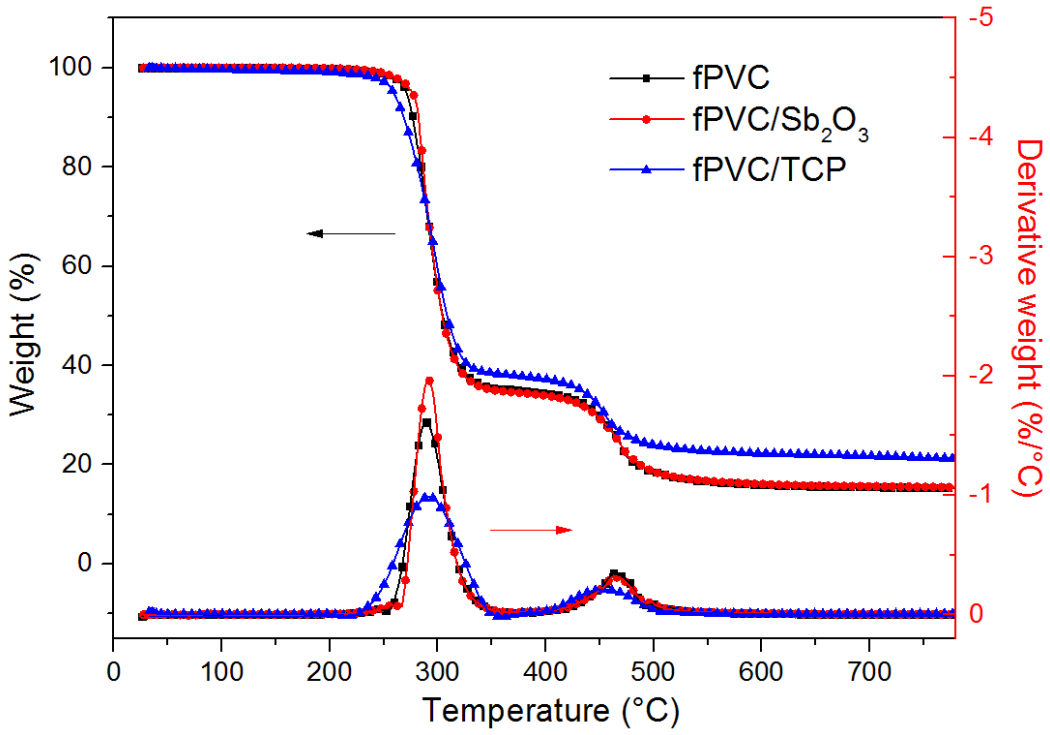

Fig. 6 TGA and DTG profiles of flexible PVC composites in N_2 gas.

Table 1 TGA and DTG results of flexible PVC composites

Sample	$T_{5\%}$ (°C)	T_{max1} (°C)	T_{max2} (°C)	Residue at 780°C (wt.%)
fPVC	271	289	465	15.4
fPVC/Sb_2O_3	277	291	463	15.5
fPVC/TCP	259	292	455	21.2

3.3. Fire and smoke hazards of flexible PVC composites

Limiting oxygen index (LOI) test and vertical burning test (UL-94) are extensively exploited to estimate the flame retardancy of polymer composites [28]. The corresponding data of flexible PVC composites are tabulated in Table 2. The LOI value of fPVC was 25%. The value increased to 34.5% with the help of Sb_2O_3 while that of fPVC containing TCP achieved nearly the same level. For UL-94 test, the conventional thickness of the test sheets is not suitable due to the intrinsic flame retardancy of fPVC composite: even the pristine sample can pass V-0 rating with the thickness of 3.2 mm. In this research, 0.6 mm thickness was adopted for the sample sheets to implement UL-94 test to monitor the distinctions between different samples. During the test, the burning speed of pure fPVC was fast once ignited, and only one ignition the flame reached to clamp which meant the sample sheet was exhausted with no rating. With the help of Sb_2O_3, the composite burned slowly and finally passed V-0 rating, however, the dripping behavior happened (not ignite the cotton). The condition became better for the case of TCP, the specimen also reached a V-0 rating and dripping was avoided. The

dripping phenomenon of fPVC/Sb_2O_3 sample was probably because of the brittle char layer generated during burning process, which was too weak to keep the char complete. On the contrary, the char of TCP-treated sample was considerably tough and compact because of the contribution of SnO_2 in the condensed phase thus this sample featured best fire behavior. In summary, the addition of TCP improved the LOI value of the composite by 10%, and helped the composite pass V-0 rating for UL-94 test without dripping, illuminating that fire hazard of the composite was lowered efficiently.

Table 2 LOI and UL-94 details of flexible PVC composites

Sample	LOI (%)	UL-94 (0.6 mm)	Dripping behavior	Flame to clamp
fPVC	25.0	No rating	Yes	Yes
fPVC/Sb_2O_3	34.5	V-0	Yes	No
fPVC/TCP	35.0	V-0	No	No

For various situations, cone calorimeter test is regarded to be the relative crucial test, herein, heat release rate (HRR), total heat release (THR), total smoke production (TSP) and mass loss were monitored to detect the fire performance of composites [29]. The data attained from cone calorimeter were recorded in Table 3.

Table 3 Cone calorimeter data summary of flexible PVC composites

Parameter	Sample		
	fPVC	fPVC/Sb_2O_3	fPVC/TCP
TTI (s)	20 ± 1	25 ± 1	26 ± 0
PHRR (kW/m^2)	218 ± 9	192 ± 3	161 ± 4
THR (MJ/m^2)	81 ± 4	84 ± 2	55 ± 2
TSP (m^2)	23 ± 1	21 ± 1	15 ± 1
Av-EHC (MJ/kg)	16.1 ± 0.8	16.8 ± 1.1	19.3 ± 0.5
Char residue (wt.%)	12 ± 1	10 ± 2	23 ± 1
Cl^- concentration (μg/ml)	58 ± 6	53 ± 4	34 ± 2

In the course of the test, time to ignition (TTI) means the time needed for the specimen to ignite within the heat flux of a cone calorimeter [30]. In this case, pure fPVC spent 20 ± 1 s to be ignited while the sample containing Sb_2O_3 and TCP prolonged the TTI to around 25 s. The HRR curves depicted in Fig. 7 conveyed that the fPVC composites burnt fiercely once ignited, indicating its vulnerable property to the fire. The PHRR emerged at the early stage in the time range 20-50 s, and this sharp peak represented the extent of fire hazards attached to each sample. The PHRR value of pristine fPVC was 218 ± 9 kW/m^2, while after adding Sb_2O_3 into the system, the PHRR value deceased to 192 ± 3 kW/m^2, whereas the PHRR value of fPVC/TCP further reduced to 161 kW/m^2, with a 23% decrease in comparison to that of the pure one. In addition, whole curve for fPVC/TCP was below the other two curves,

manifesting much milder combustion process and less potential fire hazards. In contrast, the curves of the rest two samples both gave rise to additional peaks with the height equal to the first one, verifying the poor ability of char formation. From this important graph, the tendencies of heat release were characteristic for these two flame retardants: Sb_2O_3 acted in gas phase and TCP mainly worked in condensed phase.

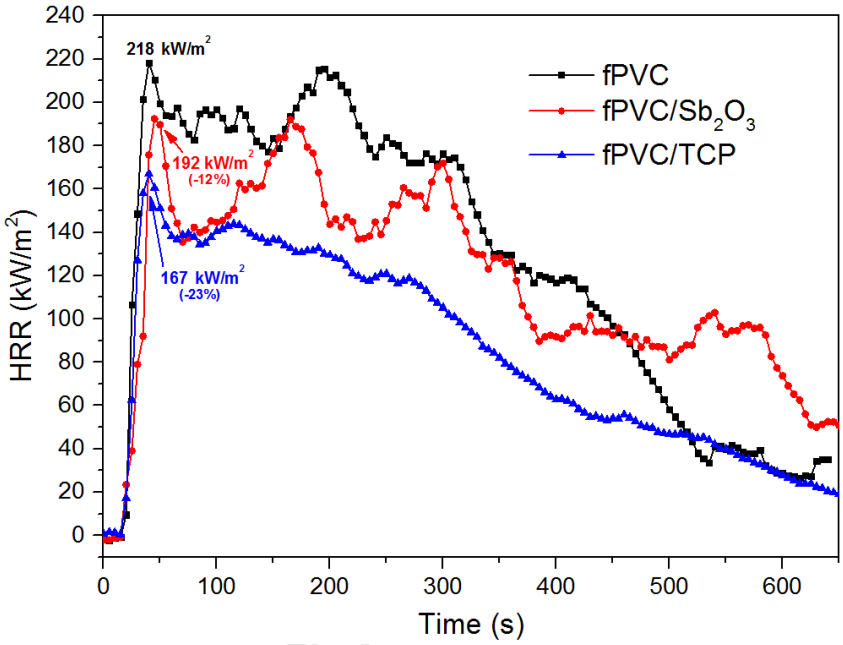

Fig. 7 Heat release rates of fPVC composites under the heat flux of 50 kW/m^2.

Additionally, the THR curves were portrayed in Fig. 8. It can be seen that when the time went to 640 s, the THR value (81 ± 4 MJ/m^2) of fPVC was greatly higher than that of other samples. The gradient of THR curve may be regarded as the representation of flame spread [31]. The gradient of THR curve from fPVC/Sb_2O_3 reduced, exhibiting the slowdown of the flame spread speed. For the sample containing TCP, the flame spread further decreased. It might be explained with assumption that much more expandable and robust char layer producing upon the sample, obstructing the fire extension. Note furthermore the average effective heat of combustion (Av-EHC)

presented in Table 3. The Av-EHC measures the heat from the combustion of combustible gases evolved. A flame retardant exhibiting flame inhibition in the gaseous phase would lead to incomplete combustion of the volatilized materials, thus the corresponding composite owns relatively low Av-EHC. On the contrary, an increased Av-EHC indicates a condensed phase effect in flame retardant [32]. The Av-EHC of fPVC/TCP was higher than that of fPVC/Sb_2O_3, suggesting that TCP mainly presented condensed phase effect in the composite, while Sb_2O_3 mainly functioned in the gaseous phase. It also implied that the formation of the potent smoke-formers, aromatics were inhibited which corresponded to the formation of more aliphatic fragments in presence of TCP, thus leading to less smoky.

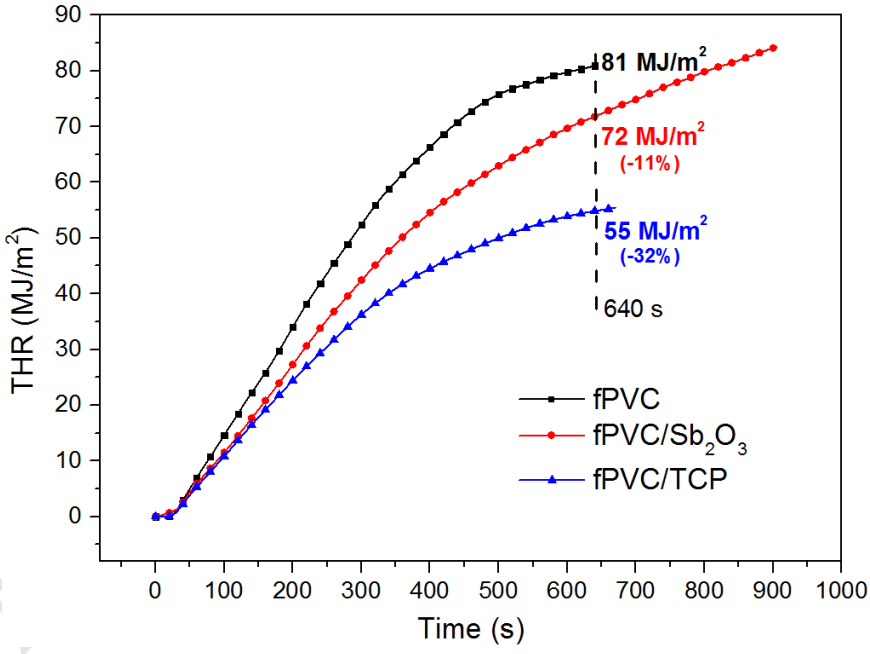

Fig. 8 Total heat release of fPVC composites under the heat flux of 50 kW/m^2.

The smoke hazards were reflected by monitoring the TSP under the heat flux of 50 kW/m^2 in the cone calorimeter test. The results were shown in Fig. 9. It obviously took on a significant decrease with the help of the flame retardants. The distinction between

the untreated fPVC composite and the flame retarded samples became apparent after 200 s. When the experiments finished, the TSP of fPVC and fPVC/Sb_2O_3 were 23 ± 1 m^2 and 21 ± 1 m^2, respectively. Nevertheless, the TSP value for fPVC/TCP was merely 15 ± 1 m^2, with 35% lower than that of the pure sample. The great decrease of TSP value with the addition of TCP was because of the smoke suppression properties of TCP. The reason was probably that TCP promoted the generation of robust char layer to hamper combustible volatiles from emitting to the air. Now that surface area of flame retardant might play a vital role in cone calorimeter test, the porous microstructure of TCP with enlarged specific surface area made O_2 and flammable volatiles trap in the channel, resulting in low heat release and smoke production. Likewise, the free radicals might enter into the pores and quench to slow down the combustion. The further explanation will be demonstrated in the next part in combination with the mass loss.

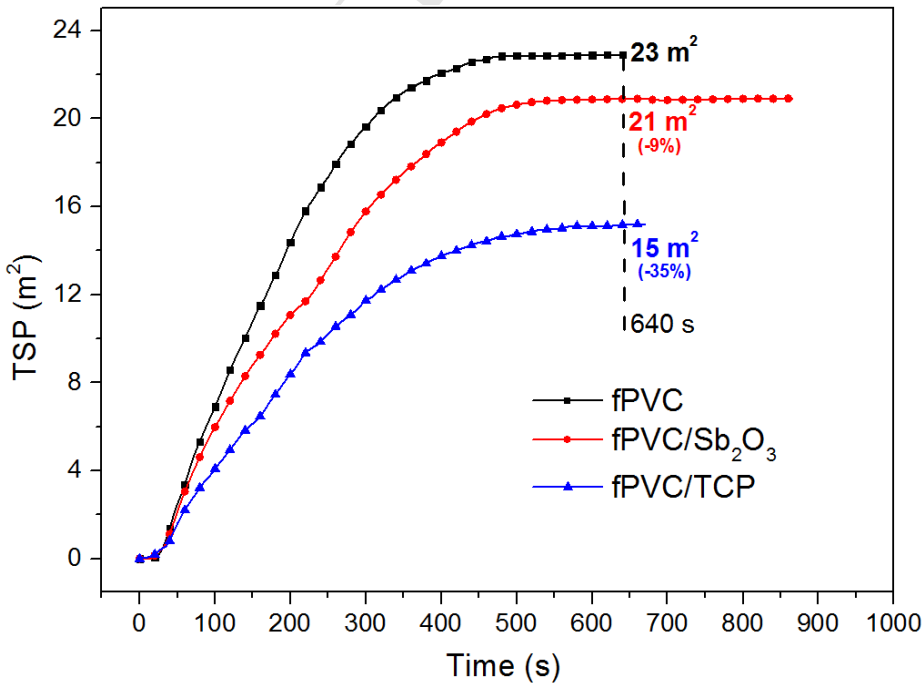

Fig. 9 Total smoke production of fPVC composites under the heat flux of 50 kW/m^2.

Fig. 10 gave the mass loss curve as a function of time for the specimens. It can be easily observed that the mass losses for fPVC and fPVC/Sb_2O_3 were very large, only around 10% remained at the end of the test. But in the case of TCP containing sample, more than 20% residue was left. In the course of burning, char might exist on the surface of the sample, generating a physical prohibition layer for heat and mass transfer. The barrier prevented O_2 from penetrating into the substrate beneath or gave the slow volatilization rate. The mass loss performance was in consistence with the performance of heat release and smoke production. The reduction in mass loss was ascribed to char formation and its morphological structure on the surface of the composites [33]. The continuous and robust char layer formed in the cone calorimeter test managed to hinder heat to the hidden material and combustible volatiles into flame zone, leading to a large char residue amount.

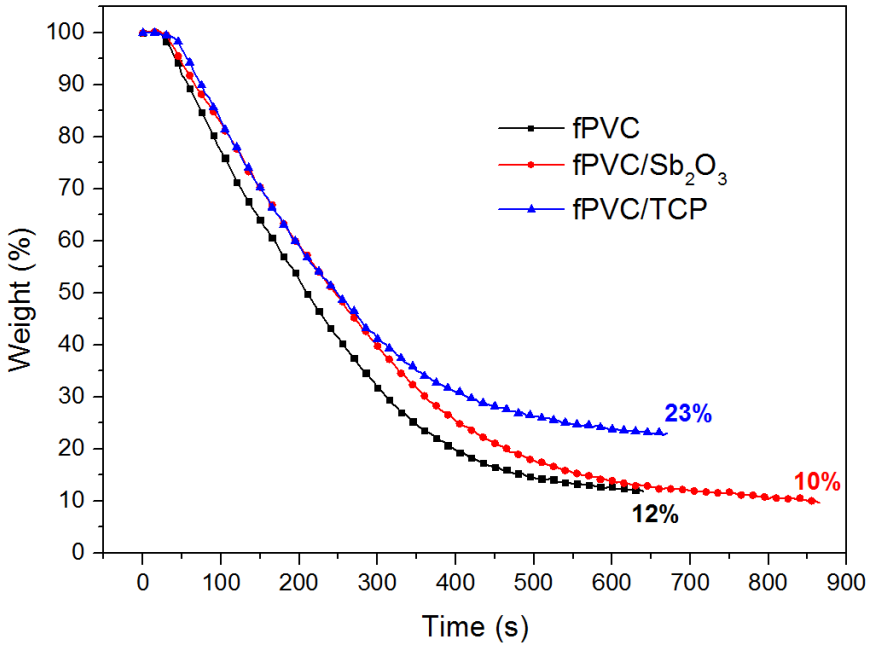

Fig. 10 Mass loss curves of fPVC composites under the heat flux of 50 kW/m^2.

The most worthy noting was that the HCl amounts evolved from fPVC composites

during combustion were measured and compared with each other among all the samples in this research. By reason of the toxic and corrosive features, the evolution of HCl gas is assumed to be another risk during the combustion of fPVC composite. The addition of TCP almost reduced by half of the Cl^- content in the solution from 58 ± 6 μg/ml to 34 ± 2 μg/ml, suggesting the decrease of HCl gas amount during the cone calorimeter test. It is already reported massively that the calcium-based compounds are very effective for the removal of HCl by virtue of the reaction to form calcium chloride which finally remained in the condensed phase [18]. The mesopores in the structure facilitated the interaction with evolved HCl gas.

To further comprehend the structure of char layers, the char morphology were studied by SEM (Fig. 11). There were many holes and crevices in the surface of fPVC sample that provided pathway for the release of smoke particles, combustible pyrolysis products and formed thermal. The char layer of fPVC/Sb_2O_3 had the similar situation and appeared exceedingly brittle. Amazingly, the introduction of TCP into the composite resulted in a continuous, expansive and compact char layer without any visible pores. The small particles on the char layer might be the calcium/tin-based chlorides. This can be explained that TCP helped to improve charring and forming dense char layer, inhibiting the heat release and smoke formation.

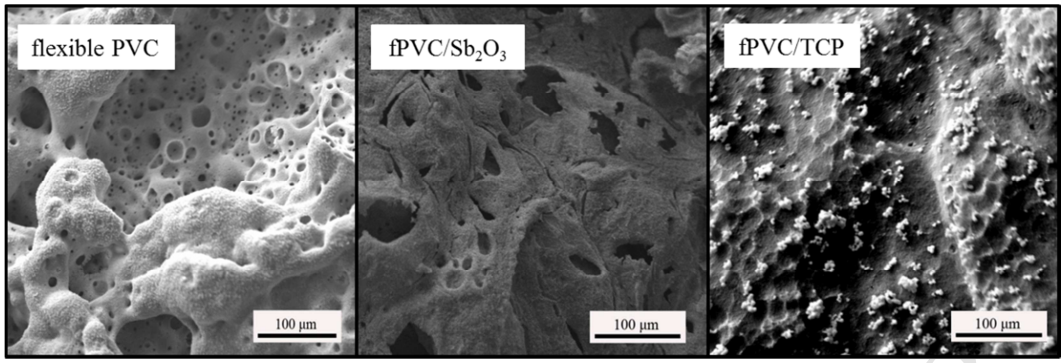

Fig. 11 SEM graphics of residues from fPVC composites.

In summary, the mechanism (Scheme 2) for the improved flame retardancy of fPVC composite in presence of TCP was proposed as follows. At the initial stage of combustion, tin chloride as a strong Lewis acid generated by the reaction between tin oxide and hydrogen chloride, catalyzed the dehydrochlorination of the polymer chain in order to promote early cross-linking and char formation. The dense and robust char upon the composite inhibited the discharging of heat and pyrolysis products, and prevented the polymer bulk below from forward burning. The liberated HCl gas was adsorbed by calcium pyrophosphate. The generated polyphosphoric acid rendered the dehydration of polymer matrix to form isolated char layer to protect the underneath bulk plastic. Mesoporous structure facilitated the interaction with the HCl gas and polymer matrix, meanwhile trapping the oxygen and combustible gases, quenching the free radicals in the channel, thereby leading to retard the flame [34].

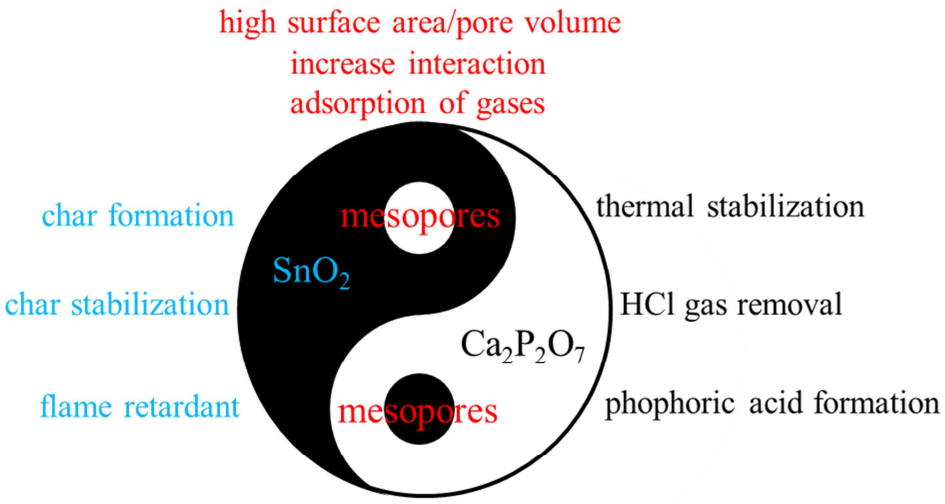

Scheme 2 Schematic illustration of the possible functions for each part of TCP in flexible PVC composite.

4. Conclusions

A novel mesoporous $SnO_2/Ca_2P_2O_7$ hybrid material was successfully prepared through several experimental steps. The chelating resin was chosen as the sustainable precursor, acting as a suitable scaffold for $SnO_2/Ca_2P_2O_7$ and offering the possibility of mesopore formation to render high specific surface area to the product. Such sustainable synthetic method has generality to fabricate $MO_x/M_yP_2O_7$ by means of choosing different adsorbed/chelated initial metal ions. The combination of $Ca_2P_2O_7$ and SnO_2 reduced significantly the fire and smoke hazards of fPVC and decreased the amount of hazardous HCl gas release during combustion. Importantly, based on the fire tests, the TCP behaved better performance than Sb_2O_3 which meant this novel flame retardant had great potential to totally replace Sb_2O_3 and offered a promising approach to develop sustainable Sb_2O_3-free fPVC composite with low fire hazard in practical application.

Acknowledgments

This research is funded by Spanish Ministry of Economy and Competitiveness (MINECO) under Ramón y Cajal fellowship (RYC-2012-10737), PhD program funded by China Scholarship Council (201306120037) and COST Action CM1302 (Smart Inorganic Polymers).

References

[1] X. Xiao, Z. Zeng, S. Xiao, Behavior and products of mechano-chemical dechlorination of polyvinyl chloride and poly (vinylidene chloride), J. Hazard. Mater. 151 (2008) 118-124.
[2] X.-Y. Bai, Q.-W. Wang, S.-J. Sui, C.-S. Zhang, The effects of wood-flour on combustion and thermal degradation behaviors of PVC in wood-flour/poly (vinyl chloride) composites, J. Anal. Appl. Pyrol. 91 (2011) 34-39.
[3] H. Qu, W. Wu, Y. Zheng, J. Xie, J. Xu, Synergistic effects of inorganic tin compounds and Sb_2O_3 on thermal properties and flame retardancy of flexible poly (vinyl chloride), Fire Safety J. 46 (2011) 462-467.
[4] D. Wang, Q. Zhang, K. Zhou, W. Yang, Y. Hu, X. Gong, The influence of manganese-cobalt oxide/graphene on reducing fire hazards of poly (butylene terephthalate), J. Hazard. Mater. 278 (2014) 391-400.
[5] Y. Liu, J.-C. Zhao, C.-J. Zhang, Y. Guo, P. Zhu, D.-Y. Wang, Effect of manganese and cobalt ions on flame retardancy and thermal degradation of bio-based alginate films, J. Mater. Sci. 51 (2016) 1052-1065.
[6] W. Tang, L. Song, S. Zhang, H. Li, J. Sun, X. Gu, Preparation of thiourea-intercalated kaolinite and its influence on thermostability and flammability of polypropylene composite, J. Mater. Sci. 52 (2017) 208-217.
[7] X. Chen, Y. Jiang, C. Jiao, Smoke suppression properties of ferrite yellow on flame retardant thermoplastic polyurethane based on ammonium polyphosphate, J. Hazard. Mater. 266 (2014) 114-121.
[8] F. Lestari, A. Green, G. Chattopadhyay, A.J. Hayes, An alternative method for fire smoke toxicity assessment using human lung cells, Fire Safety J. 41 (2006) 605-615.
[9] Y. Alarie, Toxicity of fire smoke, Crit. Rev. Toxicol. 32 (2002) 259-289.
[10] R.M. Lum, MoO_3 additives for PVC: a study of the molecular interactions, J. Appl. Polym. Sci. 23 (1979) 1247-1263.
[11] S. Saracoglu, M. Soylak, M. Dogan, L. ELCI, Speciation of antimony using chromosorb 102 resin as a retention medium, Anal. Sci. 19 (2003) 259-264.
[12] Y.-T. Pan, C. Trempont, D.-Y. Wang, Hierarchical nanoporous silica doped with tin as novel multifunctional hybrid material to flexible poly (vinyl chloride) with greatly improved flame retardancy and mechanical properties, Chem. Eng. J. 295 (2016) 451-460.

[13] Y.-T. Pan, X. Wang, Z. Li, D.-Y. Wang, A facile approach towards large-scale synthesis of hierarchically nanoporous SnO_2@Fe_2O_3 0D/1D hybrid and its effect on flammability, thermal stability and mechanical property of flexible poly (vinyl chloride), Compos. Part B-Eng 110 (2017) 46-55.
[14] Y.-T. Pan, D.-Y. Wang, Fabrication of low-fire-hazard flexible poly (vinyl chloride) via reutilization of heavy metal biosorbents, J. Hazard. Mater. 339 (2017) 143-153.
[15] S. Dahiya, B. Singh, S. Gaur, V. Garg, H. Kushwaha, Analysis of groundwater quality using fuzzy synthetic evaluation, J. Hazard. Mater. 147 (2007) 938-946.
[16] S. Abo-Farha, A. Abdel-Aal, I. Ashour, S. Garamon, Removal of some heavy metal cations by synthetic resin purolite C100, J. Hazard. Mater. 169 (2009) 190-194.
[17] L. Dong, C. Hu, L. Song, X. Huang, N. Chen, L. Qu, A large-area, flexible, and flame-retardant graphene paper, Adv. Funct. Mater. 26 (2016) 1470-1476.
[18] T. Karayildirim, J. Yanik, M. Yuksel, M. Saglam, C. Vasile, H. Bockhorn, The effect of some fillers on PVC degradation, J. Anal. Appl. Pyrol. 75 (2006) 112-119.
[19] H. Zhu, X. Jiang, J. Yan, Y. Chi, K. Cen, TG-FTIR analysis of PVC thermal degradation and HCl removal, J. Anal. Appl. Pyrol. 82 (2008) 1-9.
[20] H. Nakagawa, K. Watanabe, Y. Harada, K. Miura, Control of micropore formation in the carbonized ion exchange resin by utilizing pillar effect, Carbon 37 (1999) 1455-1461.
[21] Z. Li, M. Shao, L. Zhou, R. Zhang, C. Zhang, M. Wei, D.G. Evans, X. Duan, Directed growth of metal-organic frameworks and their derived carbon-based network for efficient electrocatalytic oxygen reduction, Adv. Mater. 28 (2016) 2337-2344.
[22] S. Wang, M. Chen, Y. Xie, Y. Fan, D. Wang, J.J. Jiang, Y. Li, H. Grützmacher, C.Y. Su, Nanoparticle cookies derived from metal-organic frameworks: Controlled synthesis and application in anode materials for lithium-ion batteries, Small 12 (2016) 2365-2375.
[23] Y. Wang, J. Zhang, Thermal stabilities of drops of burning thermoplastics under the UL 94 vertical test conditions, J. Hazard. Mater. 246 (2013) 103-109.
[24] Y.-T. Pan, D.-Y. Wang, One-step hydrothermal synthesis of nano zinc carbonate and its use as a promising substitute for antimony trioxide in flame retardant flexible poly(vinyl chloride), RSC Adv. 5 (2015) 27837-27843.
[25] X. Feng, W. Xing, L. Song, Y. Hu, K.M. Liew, TiO_2 loaded on graphene nanosheet as reinforcer and its effect on the thermal behaviors of poly (vinyl chloride) composites, Chem. Eng. J. 260 (2015) 524-531.
[26] S. Vadukumpully, J. Paul, N. Mahanta, S. Valiyaveettil, Flexible conductive graphene/poly (vinyl chloride) composite thin films with high mechanical strength and thermal stability, Carbon 49 (2011) 198-205.
[27] P. Jia, M. Zhang, L. Hu, G. Feng, C. Bo, Y. Zhou, Synthesis and application of environmental castor oil based polyol ester plasticizers for poly (vinyl chloride), ACS Sustain. Chem. Eng. 3 (2015) 2187-2193.
[28] H. Ge, G. Tang, W.-Z. Hu, B.-B. Wang, Y. Pan, L. Song, Y. Hu, Aluminum hypophosphite microencapsulated to improve its safety and application to flame retardant polyamide 6, J. Hazard. Mater. 294 (2015) 186-194.

[29] C. Li, J. Wan, Y.-T. Pan, P.-C. Zhao, H. Fan, D.-Y. Wang, Sustainable, biobased silicone with layered double hydroxide hybrid and their application in natural-fiber reinforced phenolic composites with enhanced performance, ACS Sustain. Chem. Eng. 4 (2016) 3113-3121.
[30] H.-B. Chen, Y.-Z. Wang, D.A. Schiraldi, Preparation and flammability of poly (vinyl alcohol) composite aerogels, ACS Appl. Mater. Inter. 6 (2014) 6790-6796.
[31] C. Jiao, X. Chen, Flammability and thermal degradation of intumescent flame-retardant polypropylene composites, Polym. Eng. Sci. 50 (2010) 767-772.
[32] J. Feng, J. Hao, J. Du, R. Yang, Using TGA/FTIR TGA/MS and cone calorimetry to understand thermal degradation and flame retardancy mechanism of polycarbonate filled with solid bisphenol A bis (diphenyl phosphate) and montmorillonite, Polym. Degrad. Stabil. 97 (2012) 605-614.
[33] M. Lin, B. Li, Q. Li, S. Li, S. Zhang, Synergistic effect of metal oxides on the flame retardancy and thermal degradation of novel intumescent flame-retardant thermoplastic polyurethanes, J. Appl. Polym. Sci. 121 (2011) 1951-1960.
[34] Y.-T. Pan, L. Zhang, X. Zhao, D.-Y. Wang, Interfacial engineering of renewable metal organic framework derived honeycomb-like nanoporous aluminum hydroxide with tunable porosity, Chem. Sci. 8 (2017) 3399-3409.